Kinetics of Oxygen Exchange over CeO_2-ZrO_2 Fluorite-Based Catalysts

Ekaterina M. Sadovskaya,*,† Yulia A. Ivanova,† Larisa G. Pinaeva,† Giacomo Grasso,‡ Tatiana G. Kuznetsova,† Andre van Veen,‡ Vladislav A. Sadykov,† and Claude Mirodatos*,‡

Boreskov Institute of Catalysis SB RAS, Pr. Lavrientieva 5, 630090, Novosibirsk, Russia, and Institut de Recherches sur la Catalyse et l'Environnement de Lyon−IRCELYON, UMR 5256 CNRS/ Université Lyon 1, 2 Avenue Albert Einstein, F-69626 Villeurbanne Cedex, France

Received: December 20, 2006; In Final Form: March 5, 2007

The kinetics of $^{18}O/^{16}O$ isotopic exchange over $CeO_2-ZrO_2-La_2O_3$ and Pt/CeO_2-ZrO_2 catalysts have been investigated under the conditions of dynamic adsorption−desorption equilibrium at atmospheric pressure and a temperature range of 650−850 °C. The rates of oxygen adsorption−desorption on Pt sites, support surface, oxygen transfer (spillover) from Pt to the support as well as the amount of oxygen accumulated in the oxide bulk, and oxygen diffusion coefficient were estimated. The nanocrystalline structure of lanthana-doped ceria-zirconia prepared via the Pechini route with a developed network of domain boundaries and specific defects guarantees a high oxygen mobility in the oxide bulk ($D = (1.5 \div 2.0)\cdot 10^{-18}$ m^2 s^{-1} at 650 °C) and allows accumulation of over-stoichiometric/excess oxygen. For Pt/CeO_2-ZrO_2, oxygen transfer from Pt to support (characteristic time $< 10^{-2}$ s) was shown to be responsible for the fast exchange between the gas-phase oxygen and oxygen adsorbed on the mixed oxide surface. The rate of direct exchange between the gas phase and surface oxygen is increased as well due to the increased concentration (up to 2 monolayers) of surface/near subsurface oxygen species accumulated on the oxygen vacancies (originated from the incorporation of highly dispersed Pt atoms). The characteristic time of diffusion of the oxygen localized in the subsurface layers is about 1 s. The overall quantity of over-stoichiometric oxygen and/or hydroxyl groups accumulated in the bulk can reach the equivalent of 10 monolayers, and characteristic time of oxygen diffusion within the bulk is about 20 s. All these kinetic data are required for the further step of modeling partial oxidation of hydrocarbons under steady- and unsteady-state conditions.

Introduction

Fluorite-like ceria-zirconia based catalysts that combine a high oxygen storage capacity (OSC) with a metallic active phase are used in a wide range of redox-based reactions.[1−3] Within the perspective of new domains of application like domestic hydrogen production from diverse hydrocarbons, these materials can be used for syngas generation under non-steady-state conditions and at short contact time since it corresponds to frequent operating procedures like process startup, shutdown, and fast changes in energy demand. Alternatively, this new generation of multifunctional materials is also of key importance within the area of exhaust gas treatment, especially as car exhaust gas catalysts optimized for "lean burn" conditions.

Among these catalytic materials, platinum supported on ceria-zirconia, eventually doped with other compounds like rare earth oxides, is recognized as a reference formula for its high activity and selectivity in selective oxidation of hydrocarbons to syngas.[3] The oxygen transport from the support to the metal phase is supposed to play a key role in the mechanism of this reaction and therefore deserves to be investigated carefully for getting advanced kinetics and mechanistic pathways.[4] In most cases, the dynamic oxygen mobility for similar systems was essentially characterized by techniques implemented under conditions quite different from the effective operating conditions for the selective oxidation: either $^{18}O/^{16}O$ isotopic exchange in a static reactor under low-pressure conditions[5] or under transient reducing conditions by CO pulses.[6] In addition, the above-mentioned measurements were performed in a temperature range lying far below that characterizing partial methane oxidation. In this regard, only Steady-State Isotopic Transient Analysis (SSITKA) which is per se an isotopic transient technique maintaining the overall steady state, being implemented under the exact reaction conditions, ensures the access to the right kinetic parameters.[7]

Experimental Section

Catalysts. $CeO_2-ZrO_2-La_2O_3$ (Ce:Zr:La = 0.4:0.4:0.2) mixed oxide was prepared via the Pechini route.[8] This kind of mixed oxide displays a nanocrystalline structure formed of plate-like domains with typical sizes in the range of 10−15 nm, the most developed faces being of (111) type, with a thickness in the order of nanometers. These domains are stacked into platelets with typical sizes up to 100 nm, leading to a specific surface area around 65 m^2 g^{-1}.[8] The $1.4\%Pt/CeO_2-ZrO_2-La_2O_3$ sample was prepared by adding 1.4% of Pt via incipient wetness impregnation followed by drying and calcination as described, leading to a S_{BET} value of 29 m^2 g^{-1}. The decrease in surface area after Pt addition is ascribed to the action of the acidic impregnation solution, activating the surface of Ce−Zr−O particles (hydroxylated and chlorinated). This would favor a re-stacking of the primary particles and also the incorporation of part of the Pt atoms as oxidic species within the nanodomains, forming new intercrystalline/domain boundaries, partly plugging the surface nanoporosity of the mixed oxide.[8]

SSITKA Experiments. When the steady state was achieved under $^{16}O_2$ + Ar flow over the catalyst (or the support) loaded

* Address correspondence to either author. E-mail: claude.mirodatos@ircelyon.univ-lyon1.fr (C.M.) and sadovsk@catalysis.nsk.su (E.M.S.).
† Boreskov Insitute of Catalysis SB RAS.
‡ Institut de Recherches sur la Catalyse et l'Environnement de Lyon−IRCELYON.

10.1021/jp0687706 CCC: $37.00
Published on Web 05/02/2007

into a reactor (quartz tube, i.d. = 3 mm, $L = 120$ mm), the gas mixture was replaced stepwise by the same one containing $^{18}O_2$. The transient changes in the gas isotopic composition ($^{16}O_2$, $^{16}O^{18}O$. and $^{18}O_2$ concentrations) were continuously monitored by mass spectrometry. A total of 2% vol of Ne was added into the feed gas containing the isotope molecules to ascertain whether the reactor behavior can be described as a plug-flow. The oxygen concentration in the mixture was 2% vol; the temperature was varied from 650 to 850 °C. Both the gas flow rate and catalyst loading were the same in all experiments and amounted to 200 mL min^{-1} and 0.033 g, respectively, which corresponded to a contact time of 0.01s.

Calculation Methods

Model of Isotope Exchange in a Plug-Flow Reactor. In principle, three kinetically resolvable types of isotope exchange are possible, namely, (i) homoexchange without participation of oxygen atoms of the oxide (type I characterized by corresponding rate, R^0); (ii) simple heteroexchange between one oxygen atom of gas-phase oxygen molecule and one oxygen atom of the oxide (type II, R^1); (iii) multiple heteroexchange between O_2 molecule and two oxygen atoms of the oxide (type III, R^2).[9−11] The time variation of fractions of differently labeled oxygen molecules $f_{32}(t) = (^{16}O_2)/(^{16}O_2 + {}^{16}O^{18}O + {}^{18}O_2)$, $f_{34}(t) = (^{16}O^{18}O)/(\sum{}^{i}O^{j}O)$ and $f_{36}(t) = (^{18}O_2)/(\sum{}^{i}O^{j}O)$, where $\sum{}^{i}O^{j}O = {}^{16}O_2 + {}^{16}O^{18}O + {}^{18}O_2$, is determined by the rates of all three types of exchange. The overall rate of heteroexchange $V = 0.5R^1 + R^2$ is the only factor that determines the atomic fraction of ^{18}O in gas-phase oxygen $\alpha_g(t) = (^{16}O^{18}O + 2{}^{18}O_2)/(2(^{16}O_2 + {}^{16}O^{18}O + {}^{18}O_2))$.

In turn, the atomic fraction of ^{18}O within the surface layer of the oxide ($\alpha_S(t)$) depends on the rates of both heteroexchange on the oxide surface and labeled atoms transfer in the oxide bulk. The latter can be described by a diffusion equation proposed by Klier[12] and Happel and co-workers.[13,14] In the general case accounting for the three types of exchange, the isotope exchange between the gas-phase oxygen and that in the oxide in a plug-flow reactor can be modeled on the basis of the following mass balance equations:

$$C_{O_2}\left(\frac{\partial \alpha_g}{\partial t} + \frac{1}{\tau}\frac{\partial \alpha_g}{\partial \xi}\right) = -b(0.5R^1 + R^2)(\alpha_g - \alpha_s) \qquad (1)$$

$$C_{O_2}\left(\frac{\partial f_{34}}{\partial t} + \frac{1}{\tau}\frac{\partial f_{34}}{\partial \xi}\right) = bR^0(2\alpha_g(1-\alpha_g) - f_{34}) + bR^1(\alpha_g(1-\alpha_s) + \alpha_s(1-\alpha_g) - f_{34}) + bR^2(2\alpha_s(1-\alpha_s) - f_{34}) \qquad (2)$$

$$\frac{\partial \alpha_s}{\partial t} = (0.5R^1 + R^2)(\alpha_g - \alpha_s) - \frac{N_{bulk}}{N_S}\frac{D}{h^2}\frac{\partial \alpha_{bulk}}{\partial \eta}\Big|_{\eta=0} \qquad (3)$$

Initial and boundary conditions:

$$\frac{\partial \alpha_{Obulk}}{\partial t} = \frac{D}{h^2}\frac{\partial^2 \alpha_{Obulk}}{\partial \eta^2} \qquad (4)$$

$$t = 0: \quad \alpha_g = 0, \quad f_{34} = 0, \quad \alpha_s = 0, \quad \alpha_{bulk} = 0$$

$$\xi = 0: \quad \alpha_g = \alpha_g^{input}, \quad f_{34} = f_{34}^{input}$$

$$\eta = 0: \quad \alpha_{bulk} = \alpha_s$$

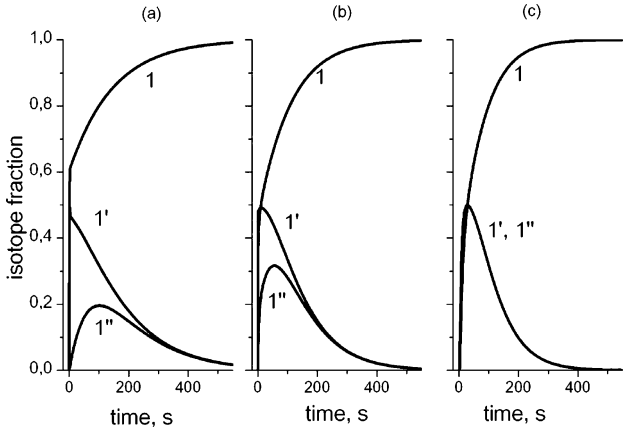

Figure 1. $\alpha_g(t)|_{\xi=1}$ (curve 1) and $f_{34}(t)|_{\xi=1}$ (curves 1′, 1″) as a function of time on stream, as calculated according to the different mechanisms of exchange (1′, type II; 1″, type III) at different ratios between the rate of heteroexchange and diffusion coefficient: (a) $V \ll D/(\Delta h)^2$, (b) $V = D/(\Delta h)^2$, (c) $V \gg D/(\Delta h)^2$.

Here α_g, α_S, and α_{bulk} are the atomic fractions of ^{18}O in the gas-phase oxygen, on oxide surface, and in the oxide bulk, respectively; f_{34} is the fraction of $^{16}O^{18}O$ molecule in the gas phase; C_{O_2} is the gas-phase oxygen concentration (mol/mol); τ is the residence time (s); b is the total number of surface sites (mol) per mole of gas molecules present in the catalyst section; R^0, R^1, and R^2 are the rates of different types of exchange as calculated per active site of the surface (s^{-1}); D is the diffusion coefficient of ^{18}O in the oxide bulk (m^2 s^{-1}); h is the characteristic size of oxide particle (m), N_S and N_{bulk} are the quantities of oxygen atoms on the surface and in the oxide bulk, respectively; ξ is the dimensionless reactor length; η is the dimensionless depth of oxide layer.

This model is analogous to that proposed by Klier (eqs 1, 3, and 4) for batch systems, but applied to a plug-flow reactor and supplemented by eq 2 describing the variation of the $^{16}O^{18}O$ fraction. One should note that the model of Klier was thoroughly studied, including the inverse problem solution. It was shown that by analyzing the isotope fraction $\alpha_g(t)$ variation, one can determine both the rate of heteroexchange on the oxide surface and the diffusion coefficient of labeled atoms in the bulk. By modeling the isotope exchange in a plug-flow reactor, one passes from ordinary differential equations to hyperbolic ones, which results in the change of the form of solution and can affect parametric sensitivity of the system during the inverse problem solution. In line with this, a preliminary numerical analysis of model sensitivity (eqs 1−4) solutions is provided with regard to the desired parameters (i.e., the rates of exchange (R^0, R^1, and R^2)) and the diffusion coefficient D.

The shape of calculated responses $\alpha_g(t)|_{\xi=1}$ and $f_{34}(t)|_{\xi=1}$ as a function of the ratio between the rate of interphase exchange V and that of diffusion is shown in Figure 1. Three cases can be considered:

(i) If the rate of isotope exchange is strongly determined by the heteroexchange on the oxide surface ($V \ll (D)/((\Delta h)^2)$, where $\Delta h = h\ (N_S)/(N_V)$ is the depth corresponding to one monolayer oxygen coverage), the curve representing the atomic isotope fraction $\alpha_g(t)$ as a function of time (Figure 1a, curve 1) has a break at $t = \tau$ and is close to a function of $A_0 + a(1 - e^{k(t-\tau)})$ type. In this case, the differences between the various types of exchange are pronounced. If the exchange proceeds according to mechanism II ($V = 0.5R^1$, $R^2 = R^0 = 0$), then the $^{16}O^{18}O$ fraction (Figure 1a, curve 1′) corresponds at any time to the equilibrium value $f_{34} \approx 2\alpha_g(1 - \alpha_g)$. If the exchange

proceeds according to mechanism III ($V = R^2$, $R^1 = R^0 = 0$), the $^{16}O^{18}O$ fraction (Figure 1a, curve 1″) lies substantially under its equilibrium value.

(ii) If the rate of heteroexchange is comparable with the diffusion rate ($V = (D)/((\Delta h)^2)$), the $\alpha_g(t)$ response curve is smoothed (Figure 1b) and cannot be approximated anymore by an exponential curve. The kinetic distinctions between the different types of mechanisms tend to decrease.

(iii) In the extreme case where the rate of isotope exchange is determined only by ^{18}O diffusion in the oxide bulk ($V \gg (D)/((\Delta h)^2)$), all differences between the various mechanisms of exchange vanish (Figure 1c).

Thus, the above calculations clearly demonstrate the high sensitivity of the dynamics of isotope response in the plug-flow reactor with regard to the relative rates of interphase exchange and ^{18}O diffusion in the oxide bulk. Note especially that the ratio between V and D influences not only $\alpha_g(t)$ dependence but also $f_{34}(t)$. At such, in the case of exchange of type III, which is most typical for oxides,[11,15] the sensitivity of $f_{34}(t)$ is even higher than that of $\alpha_g(t)$. In particular, the maximal value of $f_{34}(t)$ depends prominently on the V/D ratio (Figure 1).

Modeling of Experimental Transient Isotope Concentration Curves. The numerical analysis of the SSITKA curves, which corresponds to the solution of the inverse problem of the system of eqs 1−4 was carried out through the minimization of the next objective functional:

$$F(\bar{\vartheta}) = \left(\int_o^{t_{end}} (\alpha_g^{calc}(t, \bar{\vartheta}) - \alpha_g^{exp}(t))^2\, dt + \int_o^{t_{end}} (f_{34}^{calc}(t, \bar{\vartheta}) - f_{34}^{exp}(t))^2\, dt\right) \rightarrow \min$$

where $\alpha_g^{exp}(t)$ and $f_{34}^{exp}(t)$ are the experimental and $\alpha_g^{calc}(t, \bar{\vartheta})$ and $f_{34}^{calc}(t, \bar{\vartheta})$ are the calculated dependencies of the isotope fractions in the gas-phase oxygen at the reactor outlet.

Data Fitting. For evaluating the quality of the fit between experimental transient curves and the calculated ones, the least-square deviation was evaluated as follows:

$$Sq = \left(\sum_{i=1}^{N} (\alpha_i^{calc} - \alpha_i^{exp})^2/N + \sum_{i=1}^{N} (f_{34\ i}^{calc} - f_{34\ i}^{exp})^2/N\right)^{1/2}$$

where N is the number of experimental points. Two time intervals were considered (10−150 and 10−550 s) to emphasis larger deviation for the initial period of the transient curves.

Results

Experimental Isotopic Transient Curves. Figure 2 presents data on the isotope fractions $\alpha_g(t)$ and $f_{34}(t)$ versus time on stream as measured in SSITKA experiments over both $CeO_2-ZrO_2-La_2O_3$ and $Pt/CeO_2-ZrO_2-La_2O_3$ samples at 650 (Figure 2a) and 850 °C (Figure 2b).

$CeO_2-ZrO_2-La_2O_3$ System. By comparing $\alpha_g(t)$ and $f_{34}(t)$ experimental curves observed over $CeO_2-ZrO_2-La_2O_3$ with the above presented models, it comes that at $T = 650$ °C (Figure 2a) the rate of oxygen exchange over the support obeys a mechanism of type III (i.e., is determined by the rate of interphase exchange; similar curve shape in Figure 1a, curves 1 and 1″ and Figure 2a, $\alpha_g(t)$ and $f_{34}(t)$). At $T = 850$ °C (Figure 2b) curve $\alpha_g(t)$ is smoothed, while the maximal value of $f_{34}(t)$ increases. As follows from model curves (vide supra), the increase of $f_{34}(t)$ maximal value results from the increase of the ratio between the rate of heteroexchange and that of label diffusion into the oxide bulk. Thus, the rate of isotope exchange onto the support surface increases faster with temperature than the rate of labeled oxygen transfer into the oxide bulk, as expected from diffusion processes less T-dependent than surface processes. The quantity of exchangeable oxygen in the support, as estimated from the difference in concentrations of labeled oxygen atoms at the reactor inlet and outlet ($N_O = (2C_{O_2}U)/(\alpha_g^{input}) \int_o^{t_{end}}(\alpha_g^{input} - \alpha_g)\, dt$) remains practically unchanged as the temperature rises and lies around $9\cdot10^{21}$ at/g.

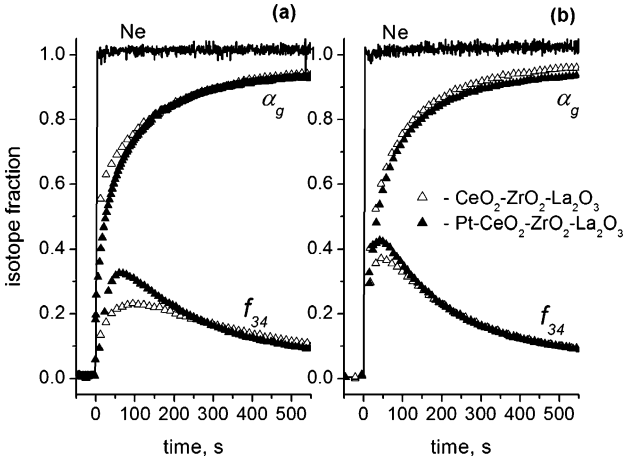

Figure 2. Experimental $\alpha_g(t)$ and $f_{34}(t)$ responses observed for $CeO_2-ZrO_2-La_2O_3$ and $Pt/CeO_2-ZrO_2-La_2O_3$ at 650 °C (a) and 850 °C (b).

$Pt/CeO_2-ZrO_2-La_2O_3$ System. From transient curves integration, the amount of exchanged oxygen during 200 s after the switch was found to be $5.3\cdot10^{21}$ at/g ($1.8\cdot10^{20}$ at/m^2) and $4.5\cdot10^{21}$ at/g ($6.8\cdot10^{19}$ at/m^2) for $Pt/CeO_2-ZrO_2-La_2O_3$ and $CeO_2-ZrO_2-La_2O_3$, respectively. It can therefore be deduced that, despite of a more than 2-fold decrease in surface area, the rate of isotope exchange over Pt-containing sample is substantially higher than that over the mixed oxide alone, especially just after the switch. Such a difference in the rates of exchange cannot be due to a fast substitution of the oxygen adsorbed on Pt, since at maximum, the concentration of the latter cannot exceed the total quantity of Pt atoms in the sample $1.5\cdot10^{18}$ at/m^2 (as calculated from Pt content in the $Pt/CeO_2-ZrO_2-La_2O_3$ sample, vide supra). The promoting effect of Pt on the observed rate of isotopic exchange has therefore to relate to the oxygen spillover between Pt and the support.

From the proximity of curves $\alpha_g(t)$ observed at 650 and 850 °C, it can be deduced that the rate of oxygen exchange over the Pt-supported catalyst increases with temperature but to a lesser extent than was observed for the support alone. However, a significant (up to the equilibrium value) increase of the fraction of mixed oxygen ($f_{34}(t)$) is observed at 850 °C. This means that, like for the support sample, the rate of oxygen exchange on the surface increases more with temperature than the labeled oxygen transfer to the bulk of the mixed oxide.

Numerical Analysis of Transient Isotope Responses. *$CeO_2-ZrO_2-La_2O_3$.* Figure 3 presents the experimental curves describing the dynamics of oxygen exchange and the curves calculated according to the different mechanisms of heteroexchange.

(i) By considering mechanism III (multiple heteroexchange between O_2 molecule and two oxygen atoms in the oxide), a good agreement is observed between experimental and calculated time dependencies of both $\alpha_g(t)$ (Figure 3a,b, curve 1) and $^{16}O^{18}O$ fraction $f_{34}(t)$ (Figure 3a,b, curve 1″), as shown from the low least-square deviation values reported in Table 1.

(ii) By considering mechanism II (simple heteroexchange between one oxygen atom of gas-phase oxygen molecule and one oxygen atom of the oxide), it can be seen that the $f_{34}(t)$

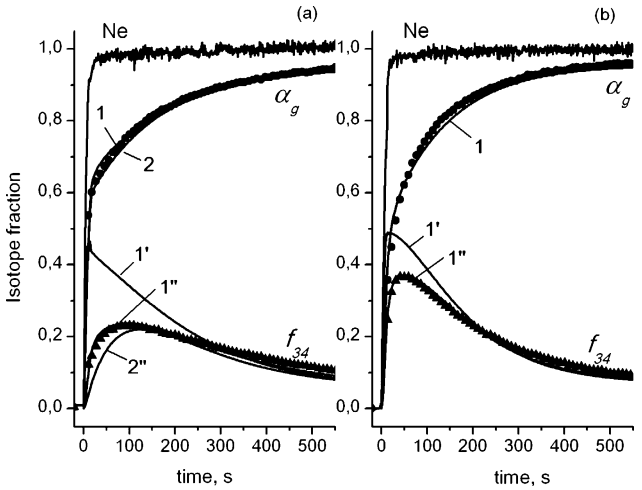

Figure 3. Calculated (lines) and experimental (points) $\alpha_g(t)$ and $f_{34}(t)$ responses over $CeO_2-ZrO_2-La_2O_3$ at 650 °C (a) and 850 °C (b). Curves 1′ and 1″ correspond to different types of mechanisms of oxygen exchange (II and III, respectively). Curves 1″ and 2″ correspond to different values of diffusion coefficient (as detailed in the text) in the case of calculation by mechanism III.

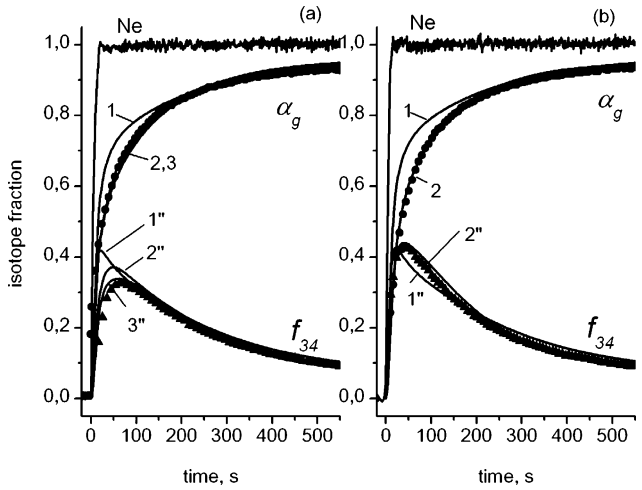

Figure 4. Calculated (lines) and experimental (points) $\alpha_g(t)$ and $f_{34}(t)$ responses over $Pt/CeO_2-ZrO_2-La_2O_3$ at 650 °C (a) and 850 °C (b). Curves 1 (1″), 2 (2″), and 3 (3″) correspond to the different values of model parameters (as detailed in the text).

TABLE 1: Least-Square Deviation Calculated between the Experimental Transient Curves and Their Calculated Models According Mechanisms II and III in Figure 3

		temperature (°C)	
time interval (s)	mechanism	650	850
10−150	III (R^2)	Sq = 0.015	Sq = 0.015
	II (R^1)	Sq = 0.102	Sq = 0.064
10−550	III (R^2)	Sq = 0.013	Sq = 0.014
	II (R^1)	Sq = 0.054	Sq = 0.035

dependence (curve 1′ in Figure 3a,b) differs substantially from the experimental one. This is confirmed by much larger least-square deviation values (Table 1), indeed more pronounced for the short time interval 10−150 s where the transient curves are far from their equilibrium values.

(iii) By adding the component describing the homoexchange (R^0) into the model a further increase of the calculated $^{16}O^{18}O$ fraction is obtained, which still worsens the fit.

Therefore, the numerical analysis has confirmed unambiguously that the isotope exchange of dioxygen with the $CeO_2-ZrO_2-La_2O_3$ material obeys a mechanism of multiple heteroexchange between O_2 molecule and two oxygen atoms of the oxide (type III, R^2).

At 650 °C, the rate of interphase exchange R^2 is the rate-determining step in the process of isotope substitution. It is obvious that in this case the sensitivity of the inverse problem solution with regard to the diffusion coefficient value is very low, so that only a lower limit of $(D)/(h^2)$ value can be estimated as <0.006 s^{-1}. As can be seen in Figure 3a, the difference between the calculated responses corresponding to $(D)/(h^2) = 0.006$ c^{-1} (curves 1 and 1″) and $(D)/(h^2) \rightarrow \infty$ (curves 2 and 2″) lies within the limit of the experimental error. In both cases the calculated rate of label transfer to the subsurface layer of the oxide $(D)/((\Delta h)^2) = (D)/(h^2)\cdot((N_{bulk})/(N_S))^2$ is substantially higher than the rate of the heteroexchange R^2. As the temperature is increased up to 850 °C, the calculated rate of interphase exchange increases and becomes comparable with that of label transfer into the subsurface layer of the oxide (Figure 3b). This gives access to a sufficiently precise estimation of both R^2 and $(D)/(h^2)$ values.

Table 2 contains the data of obtained values of R^2 as calculated per active site of the $CeO_2-ZrO_2-La_2O_3$ material (the total number of sites was set equal to the monolayer surface coverage by oxygen, i.e., $6.6\cdot10^{20}$ at/g), diffusion coefficients (as calculated for $h = V/S = 1.5\cdot10^{-8}$ m) and the intrinsic amount of exchangeable oxygen deduced from the composition of the mixed oxide. Although only the lower limit of the rate of diffusion can be determined from the experiments performed at 650 °C, the upper limits of the above-mentioned parameters are given as well, by assuming positive activation energy values and using values obtained at 850 °C.

1.4%Pt/$CeO_2-ZrO_2-La_2O_3$. For calculating the response curves in the case of $Pt/CeO_2-ZrO_2-La_2O_3$, it was first assumed that after Pt addition, the rate of oxygen exchange on the catalyst surface increases, while the rate of ^{18}O diffusion in the bulk of the mixed oxide support remains constant. All calculations have been performed on the basis of eqs 1−4. The values of diffusion coefficients D were chosen in accordance with the data presented in Table 2. Accounting for the change in the specific surface area after Pt addition (from 66 to 29 m^2 g^{-1}), h value was increased about twice as compared with $CeO_2-ZrO_2-La_2O_3$ and amounted to $3\cdot10^{-8}$ m. However, the numerical analysis has shown that by varying only the rate of oxygen exchange between the gas phase and the catalyst surface (R^2), it was impossible to describe the experimental results. The calculated rate of ^{18}O transfer to the catalysts strongly depends upon the value of diffusion coefficient and thus lies far below the experimental value. As a result, the calculated values of $\alpha_g^{calc}(t)$ exceeded substantially the experimental values obtained both at 650 °C (Figure 4a, curve 1) and at 850 °C (Figure 4b, curve 1).

In a second stage, both the diffusion coefficient D and the rate of oxygen exchange on the surface R^2 were considered as

TABLE 2: Calculated Values of the Rates of Surface Oxygen Exchange (R^2), Diffusion Coefficients (D), and Total Amount of Exchanged Oxygen ($N_{Oexchange}$) as Compared with the Intrinsic Amount of Oxygen in $CeO_2-ZrO_2-La_2O_3$ Lattice (N_{Ooxide})

T, °C	R^2, s^{-1}	R^1	R^0	D, m^2 s^{-1}	$N_{Oexchange}$, at/g	N_{Ooxide}, at/g
650	0.12 (±0.01)	0	0	1.52×10^{-18}	$9.0\ (\pm0.5) \times 10^{21}$	7.2×10^{21}
850	0.30 (±0.02)	0	0	$1.6\ (\pm0.2) \times 10^{-18}$	$9.0\ (\pm0.5) \times 10^{21}$	7.2×10^{21}

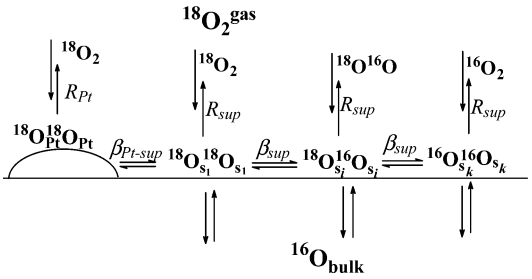

Figure 5. Scheme of gas/surface/bulk oxygen exchange on the metal and mixed oxide phase.

adjustable parameters. Calculation showed that in order to describe $\alpha_g^{exp}(t)$ for the initial period (below 100 s), the diffusion coefficient should be increased by 1 order of magnitude as compared with the value presented in Table 2. However, in this case the rate of exchange was too high for a longer time on stream. This implies that the rate of ^{18}O transfer from the surface to the mixed oxide bulk drops with depth. A detailed scheme of oxygen diffusion during the isotopic exchange within the $CeO_2-ZrO_2-La_2O_3$ mixed oxide in the absence and in the presence of Pt and the depth dependence of the diffusion coefficient will be proposed in the Discussion section.

At this stage of the modeling, by considering simply an exponential dependence of the diffusion coefficient with the mixed oxide particles depth $D(\eta) = D_0\exp(-a\eta)$ (where D_0 is the value of diffusion coefficient at $\eta = 0$), a quite good description of the dynamics of $\alpha_g^{exp}(t)$ response in all temporal intervals can now be obtained both at 650 °C (Figure 4a, curve 2) and at 850 °C (Figure 4b, curve 2). For this case, the parameters of the model are as follows:

$$R^2 = 0.6 \text{ and } 1.2 \text{ s}^{-1} \text{ at 650 and 850 °C, respectively}$$

$$D_0 = 40\cdot10^{-18} \text{ m}^2 \text{ s}^{-1},\ a = 2.3$$

(independent of temperature)

One should note that if this model adequately describes the isotopes distribution at 850 °C (Figure 4b, curve 2″), it gives obviously overestimated values of the mixed oxygen fraction $f_{34}^{calc}(t)$ at 650 °C (Figure 4a, curve 2″). As follows from the data of Galdicas et al.,[16,17] a relatively low concentration of mixed oxygen can be assigned to a gradient of ^{18}O concentration on the support surface that results from the spill-over of labeled oxygen atoms from the metallic sites to the support, as shown in Figure 5.

To take this process into account, we virtually divided the surface of the support into several parts S_i ($i = 1, ..., n$), differing by the distance from the Pt particle. The rate of isotope exchange between the neighboring parts of the support is determined by the coefficient of exchange β_{sup}, which depends on the coefficient of surface diffusion in the following manner: $\beta_{sup} = (D_{SURF})/((h_{SURF}/n)^2)$ (where D_{SURF} is the coefficient of surface diffusion, h_{SURF} is half of a distance between Pt particles, n is a number of partitioning). In accordance with the given scheme, the model of the isotope exchange can be written as follows:

$$C_{O_2}\left(\frac{\partial\alpha_g}{\partial t} + \frac{1}{\tau}\frac{\partial\alpha_g}{\partial\xi}\right) = b_{Pt}R_{Pt}{}^2(\alpha_g - \alpha_{Pt}) + \sum_{i=1}^{n}\frac{b_{sup}}{n}R_{sup}{}^2(\alpha_g - \alpha_{supi}) \quad (5)$$

$$C_{O_2}\left(\frac{\partial f_{34}}{\partial t} + \frac{1}{\tau}\frac{\partial f_{34}}{\partial\xi}\right) = b_{Pt}R_{Pt}{}^2(2\alpha_{Pt}(1-\alpha_{Pt}) - f_{34}) + \sum_{i=1}^{n}\frac{b_{sup}}{n}R_{sup}{}^2(2\alpha_{supi}(1-\alpha_{supi}) - f_{34}) \quad (6)$$

$$\frac{\partial\alpha_{Pt}}{\partial t} = R^2{}_{Pt}(\alpha_g - \alpha_{Pt}) - \beta_{Pt-sup}(\alpha_{sup1} - \alpha_{Pt}) \quad (7)$$

$$\frac{\partial\alpha_{supi}}{\partial t} = R^2{}_{sup}(\alpha_g - \alpha_{supi}) + \frac{N_{bulk}}{N_S}\frac{D}{h^2}\frac{\partial\alpha_{bulki}}{\partial\eta}|_{\eta=0} + \beta_{sup}(\alpha_{sup(i+1)} - \alpha_{supi}) + \beta_{sup}(\alpha_{sup\,(i-1)} - \alpha_{supi}) \text{ (if } i > 1) \text{ or } \beta_{Pt-sup}(\alpha_{Pt} - \alpha_{sup1}) \text{ (if } i = 1) \quad (8)$$

$$\frac{\partial\alpha_{bulki}}{\partial t} = \frac{D}{h^2}\frac{\partial^2\alpha_{bulki}}{\partial\eta^2} \quad (9)$$

Initial and boundary conditions:

$$t = 0: \quad \alpha_g = 0, \quad f_{34} = 0, \quad \alpha_{supi} = 0, \quad \alpha_{bulki} = 0$$

$$\xi = 0: \quad \alpha_g = \alpha_g^{input}, \quad f_{34} = f_{34}^{input}$$

$$\eta = 0: \quad \alpha_{bulki} = \alpha_{supi}$$

Here α_{Pt} is the fraction of ^{18}O oxygen adsorbed on Pt particles, α_{S_i} is the fraction of ^{18}O on ith part of the support surface, $R^2{}_{Pt}$ is the rate of isotope exchange between the oxygen dissociatively adsorbed on Pt and that in the gas phase, $R^2{}_{sup}$ is the rate of direct exchange between the gas-phase oxygen and that on the support surface, β_{Pt-sup} is the coefficient of exchange between the oxygen adsorbed on Pt and that localized on the adjacent to the Pt particle part of the support surface, and β_{sup} is the coefficient of the oxygen exchange between the neighboring parts of the support surface.

The numerical analysis of the model described by eqs 5−9 has shown that for a given overall rate of exchange and a given coefficient of the bulk diffusion (which are determined from the dynamics of $\alpha_g(t)$ response), the distribution of isotope oxygen molecules depends strongly on the ratio between the following parameters: $R^2{}_{sup}$, $R^2{}_{Pt}$, β_{Pt-sup}, and $D_{SURF}/h^2{}_{SURF}$.

For example, at $R^2{}_{sup}N_s \gg R^2{}_{Pt}N_{Pt}$, the gradient of ^{18}O concentration on the surface of the support approaches zero. At $R^2{}_{sup}N_s \ll R^2{}_{Pt}N_{Pt}$, the ^{18}O gradient on the support is high, but it does not affect the isotope distribution, which is determined in this case by the isotope oxygen composition on Pt particles. In both cases the calculated isotope fraction of mixed oxygen $f_{34}(t)$ does not differ from that calculated by the model described by eqs 1−4. A prominent decrease of the fraction of mixed oxygen can take place in the case of comparable contribution from both pathways (i.e., $O_2^{gas} \leftrightarrow O_{sup}$ and $O_2^{gas} \leftrightarrow O_{Pt} \leftrightarrow O_{sup}$ into the total rate of heteroexchange. Thus, the rate along the second pathway is strongly determined by the step $O_2^{gas} \leftrightarrow O_{Pt}$, because in the opposite case ($R^2{}_{Pt} > \beta_{Pt-sup}$) the fraction of mixed oxygen increases due to homoexchange on Pt sites.

Assuming the invariability of the rate of direct exchange $O_2^{gas} \leftrightarrow O_{sup}$ after Pt addition ($R^2{}_{sup} = 0.12 \text{ s}^{-1}$), namely, the second pathway (i.e., $O_2^{gas} \leftrightarrow O_{Pt} \leftrightarrow O_{sup}$) contributes mainly to the total rate of heteroexchange at 650 °C estimated as $R^2 = 0.6 \text{ s}^{-1}$. At such a ratio (1:4) between the rates along the different pathways, the calculated fraction of mixed oxygen exceeds

TABLE 3: Calculated Values of the Rates of Surface Oxygen Exchange with Pt (R^2_{Pt}) and Support (R^2_{sup}), Coefficients of Exchange between Pt and Support (β_{Pt-sup}), Diffusion Coefficients (D), and Total Amount of Exchanged Oxygen ($N_{Oexchange}$) as Compared with the Intrinsic Amount of Oxygen in the $CeO_2-ZrO_2-La_2O_3$ Lattice (N_{Ooxide})

T, °C	R^2_{Pt}, s^{-1}	β_{Pt-sup}, s^{-1}	R^2_{sup}, s^{-1}	$(D_{SURF})/(h_{SURF})$, s^{-1}	$D_0(\eta = 0)$, m^2/s	$N_{Oexchange}$, at/g	N_{Ooxide}, at/g
650	0.3 {10}[a]	≥3 {≥100}[a]	0.3(±0.02)	0.4 (±0.1)	40 (±10) × 10^{-18}	10.5 (±0.5) × 10^{21}	7.1 × 10^{21}
850	$R^2_{Pt} + R^2_{sup} = 1.2$ (±0.1)				40 (±10) × 10^{-18}	10.5 (±0.5) × 10^{21}	7.1 × 10^{21}

[a] In braces, values of R^2_{Pt} and β_{Pt-sup} as calculated per Pt atom.

substantially the observed one, similarly to that obtained by the model described by eqs 1−4. A correct description of the experimental results at 650 °C (Figure 4a, curves 3 and 3″) can be obtained only by assuming a noticeable increase of the rate of direct exchange with the support surface R^2_{sup} provided $R^2_{sup}N_{st} \approx R^2_{Pt}N_{Pt}$, $\beta_{Pt-sup} \gg R^2_{Pt}$ and $R^2_{sup} \approx D_{SURF}/h^2_{SURF}$. The corresponding values of parameters are presented in Table 3. Note especially, that the experimental value of mixed oxygen fraction is possible for this type of mechanism at a given rate of heteroexchange.

The results of the numerical analysis (eqs 5−9) for the experiments performed at 850 °C deserve additional comments. At different ratios between the parameters of the model [i.e., at (i) $R^2_{sup} < D_{SURF}/h^2_{SURF}$, $R^2_{sup}N_{st} \approx R^2_{Pt}N_{Pt}$; (ii) $R^2_{sup} \approx D_{SURF}/h^2_{SURF}$, $R^2_{sup}N_s \gg$ *(or* $\ll$*)* $R^2_{Pt}N_{Pt}$], one can obtain very close calculated fractions of mixed oxygen. They present a maximum possible at a given rate of heteroexchange and coincide with the curve calculated on the basis of the model described by eqs 1−4 (Figure 4b, curve 2). Therefore, one can state that by temperature increase from 650 to 850 °C either the rate of surface diffusion increases noticeably or the ratio between the rates of different pathways changes sharply. Taking into account that at 650 °C $R^2_{Pt} = R^2_{sup} = 0.3$ s^{-1}, while at 850 °C their summarized value $R^2_{Pt} + R^2_{sup} = 1.2$ s^{-1}, the rates of pathways cannot differ by more than three times ((1.2−0.3)/0.3 = 3). This is possible only if one of the rate values remains unchanged (activation energy is zero). The latter is highly unlikely. Therefore, we believe that the increase in the mixed oxygen fraction observed at 850 °C is mainly due to a relatively fast surface diffusion.

From the above reasoning, the following conclusions can be drawn:

(i) The oxygen exchange on the support obeys the type III mechanism (i.e., the multiple heteroexchange between one O_2 molecule and two oxygen atoms of the mixed oxide).

(ii) As the temperature rises, the rate of exchange between the gas-phase oxygen and that of the mixed oxide surface increases to a larger extent than the rate of oxygen transfer into the oxide bulk.

(iii) The quantity of exchangeable oxygen exceeds substantially the stoichiometric value (calculated in accordance with the mixed oxide composition). This excess corresponds to about 3−4 oxygen monolayers.

(iv) After Pt addition, a faster label transport appears through the spillover from Pt to the support. The rate of isotope exchange by this pathway is determined by the $O_2 \leftrightarrow PtO$ step.

(v) Pt addition affects the kinetics of direct isotope exchange between the gas-phase oxygen and that of support $O_2 \leftrightarrow O_{sup}$. Thus, the rates of both oxygen exchange on the surface and oxygen transfer in the support bulk increase. In addition, the general quantity of exchangeable oxygen increases as well.

Discussion

Oxygen Exchange over $CeO_2-ZrO_2-La_2O_3$ Mixed Oxide. *Mechanism.* As demonstrated above, in the temperature range 650−850 °C the oxygen exchange between $^{18}O_2$ and the mixed oxide surface obeys unambiguously a mechanism of type III, in agreement with earlier data of Boreskov[9] and Muzykantov et al.[10] This type of exchange considers a multistep mechanism including the step of dissociative oxygen adsorption followed by isotope exchange between the adsorbed oxygen and that of support surface. The absence of homogeneous exchange ($R^0 = 0$) is in line with the fact that adsorption/desorption steps determine the overall reaction rate. Therefore, the obtained estimation of the rate of isotope exchange R^2 and of the activation energy value can be related directly to the rates of oxygen adsorption−desorption on the surface ($r_{ads} = r_{des} = R^2$). The calculated value of the activation energy is E_{R^2}=35 kJ mol^{-1}.

Exchangeable Oxygen. Let us consider now the amount of exchangeable oxygen for the mixed oxide sample, which exceeds by several monolayers the overall amount of oxygen in the sample. About one monolayer or less can be ascribed to adsorbed oxygen; the remaining part has therefore to be ascribed to the mixed oxide bulk. It necessarily corresponds to oxygen and/or hydroxyls and/or water molecules in excess in the considered mixed oxide. Indeed, ceria-zirconia based mixed oxides prepared via the Pechini route are characterized by a nanocrystalline structure that possesses a developed network of domain boundaries, specific Frenkel-type defects, and the rearrangement of the fluorite-like structure due to changes in stoichiometry and bulk/surface cation ordering and/or segregation within the microdomains enriched by Ce or Zr, respectively.[18,19] Such disordered boundaries formed by the stacking of nanodomains were shown to promote oxygen mobility and ability to accommodate surstoichiometric oxygen[20−22] and/or hydroxyl groups. A straightforward relationship between the oxygen storage capacity in CZMO and the density of the lattice strains caused by such defects was revealed by Si et al.[23] For the oxygen isotope exchange, hydroxyls or water molecules trapped within domain boundaries could not be distinguished from the oxygen species. However, O_2 TPD data revealed that for Pt-supported Ce−Zr−La−O samples, the amount of excess oxygen desorbed into He stream does not exceed 2 monolayers.[24] Hence, hydroxyls or trapped water molecules constitute another 2−3 monolayers of exchangeable oxygen in addition to the stoichiometric pool.

Oxygen Diffusion within the Mixed Oxide. The value of oxygen diffusion coefficient within the $CeO_2-ZrO_2-La_2O_3$ mixed oxide calculated in this work deserves to be compared with data reported in the literature. The value reported by Dong et al.[5] for $Ce_{0.15}Zr_{0.85}O_2$ sample ($D = 53 \cdot 10^{-23}$ m^2 s^{-1} at 300 °C) can be extrapolated to 850 °C by using the activation energy provided by the authors ($E = 10$ kJ mol^{-1}). This gives a diffusion coefficient $D = 1.5 \cdot 10^{-21}$ m^2 s^{-1}, a value by 3 orders of magnitude lower than the value estimated in the present work ($D = 1.6 \cdot 10^{-18}$ m^2 s^{-1}). Such a difference is likely to come from a much higher concentration of defects and domain boundaries in the mixed oxide prepared via the Pechini route, as compared to the mixed oxides prepared by more conventional techniques used in.[5]

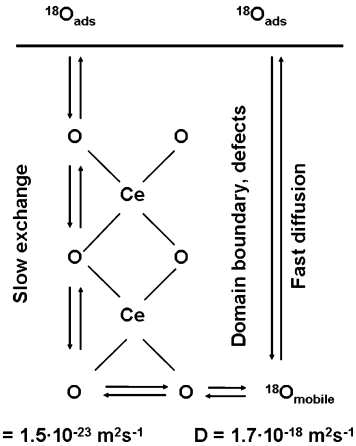

Figure 6. Scheme of oxygen diffusion during the isotopic exchange within the $CeO_2-ZrO_2-La_2O_3$ mixed oxide.

As a matter of fact, in the case of dense and regular crystalline lattice, the isotope transfer implies the exchange between neighboring oxygen atoms included into the crystalline lattice. In the defect-rich structure, dissociatively adsorbed oxygen can diffuse easily into the bulk via the defects and domain boundaries. The rate of oxygen diffusion is thus determined by the length and surface of boundaries and by the concentration of defects.

During the diffusion, atomic oxygen can exchange with the oxide domains lattice, thus resulting in the increase of the overall rate of oxygen exchange. In accordance with the above reasoning, a scheme of the isotope transfer within a defect-rich mixed oxide is presented in Figure 6.

Thus, the diffusion coefficient reported by Dong[5] would essentially be related to the process of exchange between oxygen atoms in the regular crystalline lattice, while in the present case, fast oxygen diffusion along domain boundaries combined with the internal exchange with the lattice oxygen results in a much faster overall diffusion.

One should note also that for modeling the isotope response the diffusion flow was calculated for the total amount of exchangeable oxygen in the support, while the concentration of "mobile" oxygen, equal to the difference between the quantities of exchanged oxygen ($N_{Oexchange}$) and lattice oxygen (N_{Ooxide}), amounts to about 20% (Table 2).

In this respect, the diffusion coefficient of "mobile" oxygen (D_{Omobil}) can be calculated as follows: In accordance with D,

$$D_{Omobil} \approx D\frac{O_{bulk}}{O_{mobil}} = D\frac{N_{Oexhange}}{N_{Oexhange} - N_{Ooxide}} \qquad (10)$$

$N_{Oexchange}$, and N_{Ooxide} values presented in Table 1, we obtain:

$$D_{Omobil} = 8{*}10^{-18}\ m^2 s^{-1}\ (850\ °C)$$

with an activation energy less that 7 kJ/mol, that is about five times smaller than the activation energy for the overall diffusion coefficient.

Oxygen Exchange over 1.4%Pt/$CeO_2-ZrO_2-La_2O_3$. Relatively fast processes including (i) isotope exchange between the gas-phase oxygen and oxygen adsorbed on Pt, (ii) oxygen spillover from Pt particles to the mixed oxide support and back result in a marked increase in the rate of isotope replacement for the bulk oxygen as compared to the Pt-free mixed oxide. A gradient of concentration of isotope label along the support surface has been assumed, which leads to a lower rate of the surface oxygen diffusion. This gradient affects the fractional composition of desorbing oxygen. Thus, a decrease of the mixed oxygen fraction takes place as compared with the equilibrium value. A corresponding increase of $^{16}O_2$ and $^{18}O_2$ fractions was observed. These data agree well with the results of analogous studies reported for Rh/CeO_2.[16,17]

At the same time, the increase of the rate of oxygen exchange over the Pt-containing sample cannot be simply related to the appearance of new pathways of isotope transfer (i.e., the exchange with oxygen adsorbed on Pt sites and the oxygen spillover between support and Pt). As a matter of fact, an increase of the rate of direct isotope exchange between the gas-phase oxygen and the support takes place as well (from 0.12 to 0.30 s^{-1} for R^2_{sup} at 650 °C as shown in Tables 2 and 3). Moreover, both the rate of labeled oxygen transfer to the support bulk (near subsurface layers mainly) and the overall quantity of exchangeable support oxygen are increased in the presence of Pt (from $1.6{\cdot}10^{-18}$ to $40{\cdot}10^{-18}$ $m^2\ s^{-1}$ for D and from $9{\cdot}10^{21}$ to $10.5{\cdot}10^{21}$ at/g for $N_{Oexchange}$).

Regarding the increase of the rate of gas-phase oxygen exchange with support surface (R^2_{sup}), it can be related to the increased concentration of surface/near subsurface oxygen species accumulated on the oxygen vacancies (defects) of the support. This effect would come from an electronic transfer with metal atoms,[25] especially due to the incorporation of Pt atoms into the mixed oxide lattice through the domain boundaries. This would account also for a higher amount of available oxygen from the support and the enhanced flux of oxygen along these extended defects to the surface.

Besides the formation of surface and subsurface defects, the addition of Pt also provokes a 2-fold decrease of S_{BET} value, ascribed to a restructuration of the nanodomains, the incorporation of part of the Pt atoms as oxidic species partly plugging the nanoporosity of the mixed oxide (see Catalysts section). This results in the increase of the concentration of so-called "internal" boundaries, which favors the mobility of bulk oxygen in the immediate vicinity of Pt clusters (i.e., in the near subsurface layers).

As was noted before, within the framework of the models developed in this study, the diffusion flow of labeled oxygen atoms was calculated per overall amount of exchangeable oxygen supposing its homogeneous distribution in the bulk. In fact, the empirical dependence of diffusion coefficient on the depth ($D(\eta) = D_0\ \exp(-2.3\eta)$) reflects mainly the above-discussed change of mobile oxygen concentration with depth. Note that other structural factors such as changes in Zr^{4+} ions concentration with particle depth (surface depletion) might also affect the Ce−O bond strength and, therefore, the oxygen diffusion according the particle depth. Thus, Zr^{4+} ions having a smaller ionic radius than Ce^{4+} ones, higher concentration of the former in the bulk would involve a lattice contraction and, therefore, a higher Ce−O bond strength ending up with a slower oxygen exchange.[26]

Supposing that additionally (as compared with the initial support sample) accumulated oxygen is localized preferentially in the subsurface layer ($\eta = 0-0.3$), then in accordance with eq 10, the following averaged estimates of diffusion coefficient of the "mobile" oxygen in the Pt-containing sample can be obtained for 850 °C: (i) averaged by overall support volume ($\eta = 0-1$) − $D_{Omobil} = 45{\cdot}10^{-18}$ $m^2\ s^{-1}$ and (ii) averaged by surface/near subsurface layers ($\eta = 0-0.3$) − $D_{Omobil} = 70{\cdot}10^{-18}$ $m^2\ s^{-1}$.

One should note that there is no direct correlation between the amount of oxygen adsorbed under the conditions of oxygen adsorption/desorption equilibrium (i.e., under steady-state condi-

tions) and oxygen storage capacity of the catalyst (which is evaluated under non-steady-state conditions). Thus, when switching abruptly from steady-state conditions in the presence of gas-phase oxygen to transient state by suppressing the gas-phase oxygen, oxygen adsorbed on the surface desorbs rapidly. Partial oxygen desorption from the domain boundaries takes place as well. However, as regarding the catalytic properties of fluorite-like catalysts, including partial methane oxidation reaction, the estimates of the rate of oxygen diffusion and its concentration in the support bulk are of interest since they can affect substantially the kinetics of transient regimes. The estimates of the rates of oxygen transfer from Pt to support are the most important. As was shown, oxygen spillover itself is very fast as compared with other processes determining the rate of isotope exchange (oxygen adsorption/desorption, oxygen diffusion on the surface and within the bulk of the support). The coefficient of exchange β_{Pt-sup}, estimated in this case by its lower limit, is higher than 10^2 s^{-1}. This means that the characteristic time of oxygen transfer from Pt to the support (and back) is $<10^{-2}$ s, which is comparable with the rate constants of the steps of methane oxidation over the Pt-containing catalysts.[26] At 650 °C the rate of oxygen spillover from Pt to support is determined by two processes (i.e., surface and bulk diffusion). At 850 °C the effect of the surface oxygen diffusion was not revealed. Probably, this is due to the relatively high activation energy of the rate of surface diffusion. Thus, Galdicas et al.[17] showed that the activation energy of surface diffusion over ceria-zirconia mixed oxides can reach several hundreds of kilojoules per mole. This value exceeds substantially the values related to the steps of oxygen adsorption/desorption both on Pt sites and on the support surface, and especially for bulk diffusion. The latter is close to zero. As a result, at 850 °C and above, the rate of oxygen transfer from Pt to the support is determined mainly by the oxygen diffusion within the bulk of the mixed oxide.

Conclusion

The specific structural features of ceria-zirconia based samples prepared via the Pechini route facilitate the incorporation of adsorbed oxygen and/or hydroxyls or water molecules into the bulk of the mixed oxide through domain boundaries and other defects. This amount of overstoichiometric oxygen can reach the equivalent of several monolayers, while the oxygen diffusion coefficient amounts to the value of $1.5-2$ 10^{-18} m^2 s^{-1} at 650 °C. Adding Pt to the mixed oxide results in the increase of defect concentration thus leading to a higher oxygen accumulation ability and rate of exchange. The oxygen spillover between Pt and the support originates the fast oxygen exchange observed over the Pt-containing samples. Although the characteristic time of the oxygen spillover from Pt to the support is less than 10^{-2} s at and below 650 °C, the rate of spillover is determined by the surface diffusion with a characteristic time (h^2_{SURF}/D_{SURF}) of about 2 s (at 650 °C). The rate of surface diffusion prominently increases with temperature. As a consequence, at 850 °C, the rate of spillover is determined by the diffusion into the bulk which depends weakly on temperature. The characteristic time of diffusion of the oxygen localized in the subsurface layers is about 1 s and its amount is up to 2 monolayers. The overall quantity of oxygen-containing species accumulated in the bulk can reach $3-4$ monolayers, and characteristic time of oxygen diffusion within the bulk is about 20 s.

All these intrinsic kinetic parameters related to oxygen activation and diffusion for ceria-zirconia based mixed oxide in the absence or in the presence of Pt will be used in a further transient kinetic description of the partial oxidation of methane over these reference materials.

Acknowledgment. This work was partly supported by RFBR-CNRS Project 05-03-34761.

References and Notes

(1) Otsuka, K.; Wang, Y.; Sunada, E.; Yamanaka, I. *J. Catal.* **1998**, *175*, 152.
(2) Trovarelli, A. In *Catalytic Science Series*; Hutchings, G. J., Ed.; Imperial College Press: London, 2002; Vol. 2.
(3) Mattos, L. V.; de Oliveira, E. R.; Resende, P. D.; Noronha, F. B.; Passos, F. B. *Catal. Today* **2002**, *77*, 245.
(4) Pantu, P.; Kim, K.; Gavalas, G. R. *Appl. Catal. A* **2000**, *193*, 203.
(5) Dong, F.; Suda, A.; Tanabe, T.; Nagai, Y.; Sobukawa, H.; Shinjoh, H.; Sugiura, M.; Descorme, C.; Duprez, D. *Catal. Today* **2004**, *93−95*, 827.
(6) Sadykov, V. A.; Kuznetsova, T. G.; Veniaminov, S. A.; Kochubey, D. I.; Novgorodov, B. N.; Burgina, E. M.; Moroz, E. M.; Paukshtis, E. A.; Ivanov, V. P.; Trukhan, S. N.; Beloshapkin, S. A.; Potapova, Y. V.; Lunin, V. V.; Kemnitz, E.; Aboukais, A. *React. Kinet. Catal. Lett.* **2002**, *76*, 83.
(7) Mirodatos, C. *Catal. Today* **1991**, *9*, 83.
(8) Kuznetsova, T. G.; Sadykov, V. A.; Moroz, E. M.; Trukhan, S. N.; Paukshtis, E. A.; Kolomiichuk, V. N.; Burgina, E. B.; Zaikovskii, V. I.; Fedotov, M. A.; Lunin, V. V.; Kemnitz, E. *Stud. Surf. Sci. Catal.* **2002**, *143*, 659.
(9) Boreskov, G. K. *Adv. Catal.* **1964**, *15*, 285.
(10) Muzykantov, V. S.; Popovskii, V. V.; Boreskov, G. K. *Kin. Katal.* **1964**, *5*, 624.
(11) Ozaki, A. *Isotopic Studies of Heterogeneous Catalysis*; Academic Press: New York, 1977.
(12) Klier, K.; Kucera, E. *J. Phys. Chem. Solids* **1966**, *27*, 1087.
(13) Happel, J.; Walter, E.; Lecourtier, Y. *J. Catal.* **1990**, *123*, 12.
(14) Walter, E.; Pronzato, L.; Soong, Y.; Otarod, M.; Happel, J. *Ind. Eng. Chem. Res.* **1995**, *34* (2), 483.
(15) Descorme, C.; Duprez, D. *Appl. Catal. A* **2000**, *202*, 231.
(16) Galdicas, A.; Descorme, C.; Duprez, D. *Solid State Ionics* **2004**, *166*, 147.
(17) Galdicas, A.; Duprez, D.; Descorme, C. *Appl. Surf. Sci*. **2004**, *236*, 342.
(18) Wu, X.; Fan, J.; Ran, R.; Weng, D. *Chem. Eng. J*. **2005**, *109*, 133.
(19) Perez-Omil, J. A.; Bernal, S.; Calvino, J. J.; Hernandez, J. C.; Mira, C.; Rodrıguez-Luque, M. P.; Erni, R.; Browning, N. D. *Chem. Mater*. **2005**, *17*, 4282.
(20) Boaro, M.; Trovarelli, A.; Hwang, J.-H.; Mason, T. O. *Solid State Ionics* **2002**, *147*, 85.
(21) Boaro, M.; Giordano, F.; Recchia, S.; Dal Santo, V.; Giona, M.; Trovarelli, A. *Appl. Catal. B* **2004**, *52*, 225.
(22) Saraf, L.; Wang, C. M.; Shutthanandan, V.; Zhang, Y.; Marina, O.; Baer, D. R.; Thevuthasan, S.; Nachimuthu, P.; Lindle, D. W. *J. Mater. Res.* **2005**, *20*, 1295.
(23) Si, R.; Zhang, Y. W.; Li, Sh.-J.; Lin, B.-X.; Yan, Ch.-H. *J. Phys. Chem. B*, **2004**, *108*, 12481.
(24) Sadykov, V. A.; Kuznetsova, T. G.; Yu. Frolova, V.; Alikina, G. M.; Lukashevich, A. I.; Rogov, V. A.; Muzykantov, V. S.; Pinaeva, L. G.; Sadovskaya, E. M.; Yu. Ivanova, A.; Paukshtis, E. A.; Mezentseva, N. V., L. Ch. Batuev, Parmon, V. N.; Neophytides, S.; Kemnitz, E.; Scheurell, K.; Mirodatos, C., van Veen, A. C. *Catal. Today* **2006**, *117*, 475.
(25) Frost, J. C. *Nature* **1988**, *334*, 577.
(26) Huff, M.; Torniainen, P. M.; Schmidt, L. D. *Catal. Today* **1994**, *21*, 113.
(27) Islam, M. S.; Balducci, G. In *Catalysis by Ceria and Related Materials*; Trovarelli, A.; Ed.; Catalytic Science Series; Imperial College Press: London, UK, 2002; Vol. *2*, pp 281−309.